Titanium mesh supported TiO_2 nanowire arrays/Nb-doped TiO_2 nanoparticles for fully flexible dye-sensitized solar cells with improved photovoltaic property

Wenwu Liu, Hui-gang Wang, Xiaofei Wang, Mei Zhang, Min Guo*

Table S1. The width of half height of (101) lattice plane and calculated nanoparticle size according to XRD patterns (Fig. 2(b)).

DSSCs	*Peak position* 2θ (°)	*Width of half height* *B* (°)	*Nanocrystalline size* *D* (nm)
0 mol%	25.52	0.60	13.42
1.2 mol%	25.46	0.69	11.68
2.4 mol%	25.43	0.83	9.79
4.8 mol%	25.36	0.78	10.38
9.6 mol%	25.34	0.72	11.28

School of Metallurgical and Ecological Engineering, University of Science and Technology Beijing, Beijing 100083, PR China

E-mail: guomin@ustb.edu.cn, *Fax*: 86-10-6233-4926.

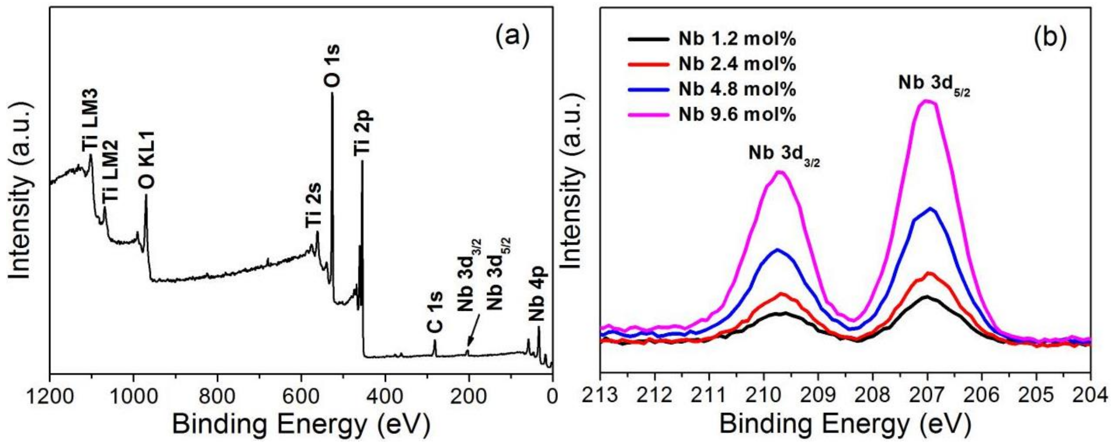

Fig. S1. (a) XPS survey spectra of Nb-doped TiO_2 NPs, and (b) Nb 3d.

For the Nb-doped TiO_2 NPs, XPS measurement was carried out and the results were presented in Fig. S1. From the full spectrum, Ti, O and Nb peaks were identified clearly. Generally, the XPS spectral peaks corresponding to the binding energies of niobium $3d_{3/2}$ and $3d_{5/2}$ electrons are often utilized to distinguish the valence state. The double peaks positioned at 209.70 and 206.90 eV confirmed that Nb^{5+} ions were indeed doped into the TiO_2 NPs.

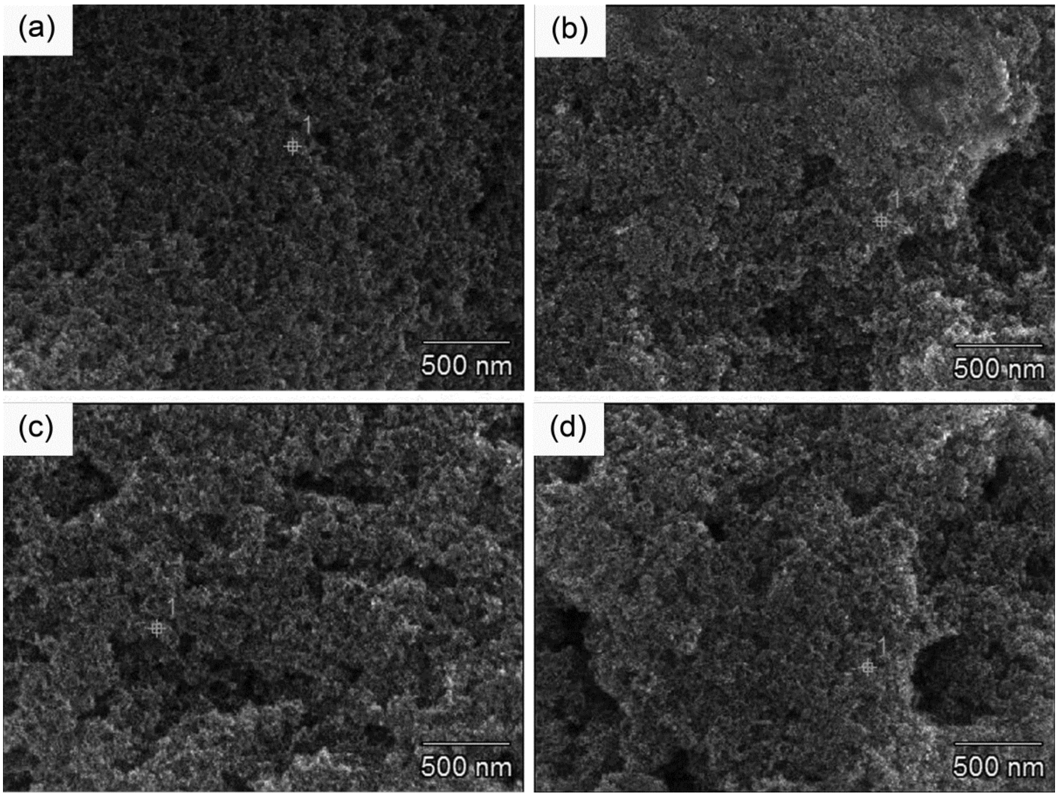

Fig. S2. FE-SEM images of the different Nb-doped TiO_2 NPs samples on FTO substrates, (a) 1.2 mol%, (b) 2.4mol%, (c) 4.8 mol%, (d) 9.6 mol%.

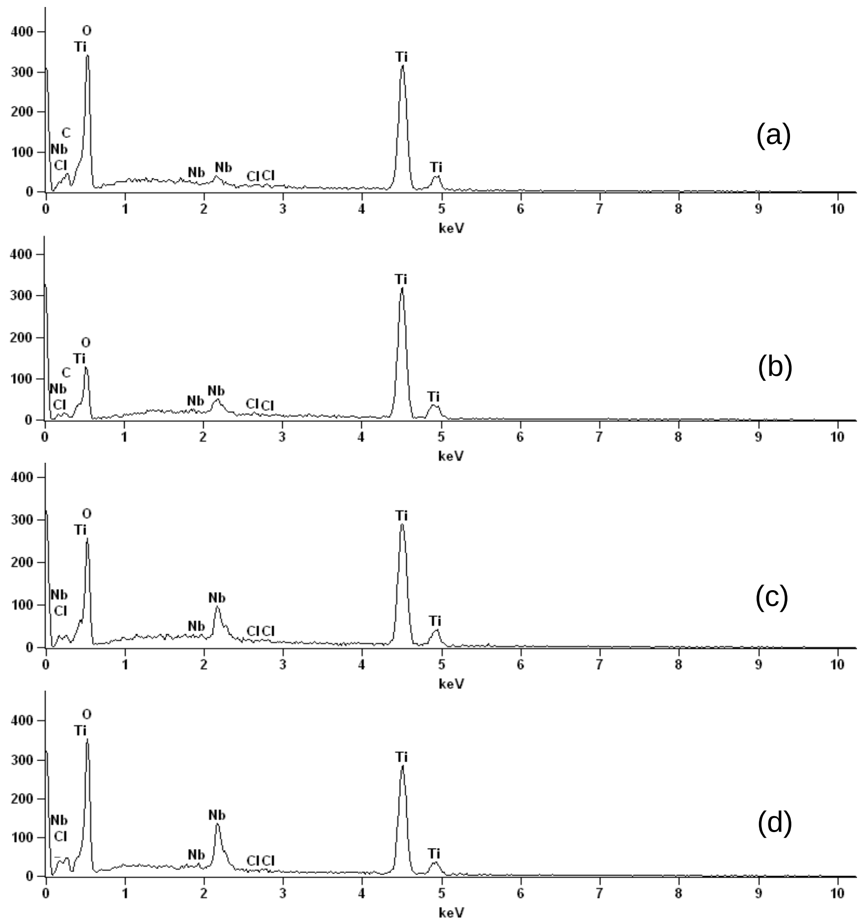

Fig. S3. EDS spectra of Nb-doped TiO_2: (a) 1.2 mol%, (b) 2.4mol%, (c) 4.8 mol%, (d) 9.6 mol%.

Table. S2. Nb doping contents of different Nb-doped TiO_2 NPs measured by EDS.

Nb doping amount (theoretical value) (mol%)	*Nb doping amount (measured by EDS)* (mol%)
1.2	1.0
2.4	2.2
4.8	4.9
9.6	9.3

Quantitative analysis of the Nb-doping amount was further performed by SEM-EDS spectra as shown in Fig S3. The experimental results summarized in Table S2 were presented to be in good agreement with the theoretical values.

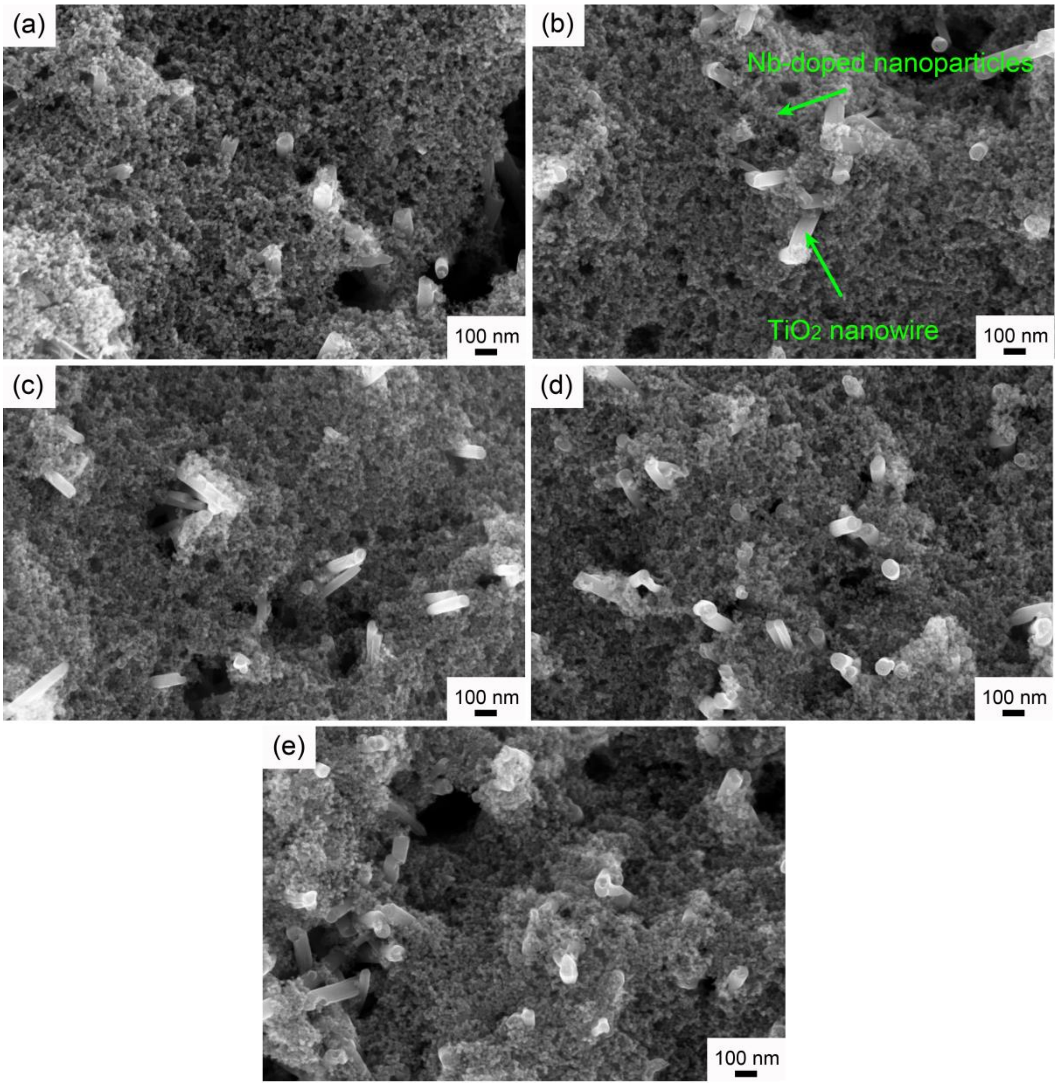

Fig. S4. Low-magnification FE-SEM images of TiO_2 NWAs/Nb-doped TiO_2 NPs on Ti mesh substrates, (a) 0 mol%, (b) 1.2 mol%, (c) 2.4 mol%, (d) 4.8 mol%, (e) 9.6 mol%.

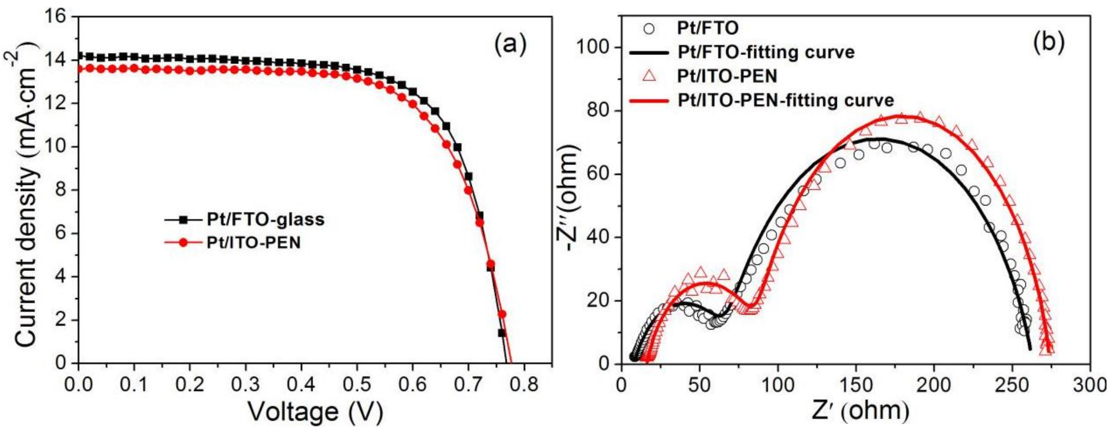

Fig. S5. Current density-voltage curves and corresponding Nyquist plots of the DSSCs based on different counter electrodes.

Table S3. Photoelectric property parameters of the DSSCs based on TiO_2 NWAs/2.4 mol% Nb-doped TiO_2 NPs photoanodes and different counter electrodes.

Counter electrode	J_{sc} (mA·cm^{-2})	V_{oc} (V)	FF	η (%)
Pt/FTO-glass	14.20	0.77	0.69	7.52
Pt/ITO-PEN	13.60	0.78	0.68	7.20

Table S4. Impedance parameters obtained by fitting actual Nyquist spectra (in the dark) of the DSSCs based on TiO_2 NWAs/2.4 mol% Nb-doped TiO_2 NPs and different counter electrodes.

Counter electrode	R_s(Ω)	R_{CE}(Ω)	R_{rec}(Ω)
Pt/FTO-glass	8.01	58.63	206.82
Pt/ITO-PEN	15.96	68.08	210.97

In order to compare the performance of DSSCs based on PEN/ITO-Pt and Glass/FTO-Pt counter electrodes, photocurrent-voltage characteristics of the DSSCs based on different counter electrode and corresponding Nyquist plots were given in Fig. S5(a-b) for comparison under similar fabrication condition, and the corresponding photovoltaic performance and fitting resistance data were summarized in Table S3-S4. The DSSC based on TiO_2 NWAs/2.4 mol% Nb-doped TiO_2 NPs photoanode and Glass/FTO-Pt counter electrode showed an higher photovoltaic efficiency (7.52%) than that of the PEN/ITO-Pt based fully flexible DSSC (7.20%), which may be ascribed to the smaller series resistance (R_s) and charge transfer resistance of the counter electrode/electrolyte interface (R_{CE}) as presented in Table S4.

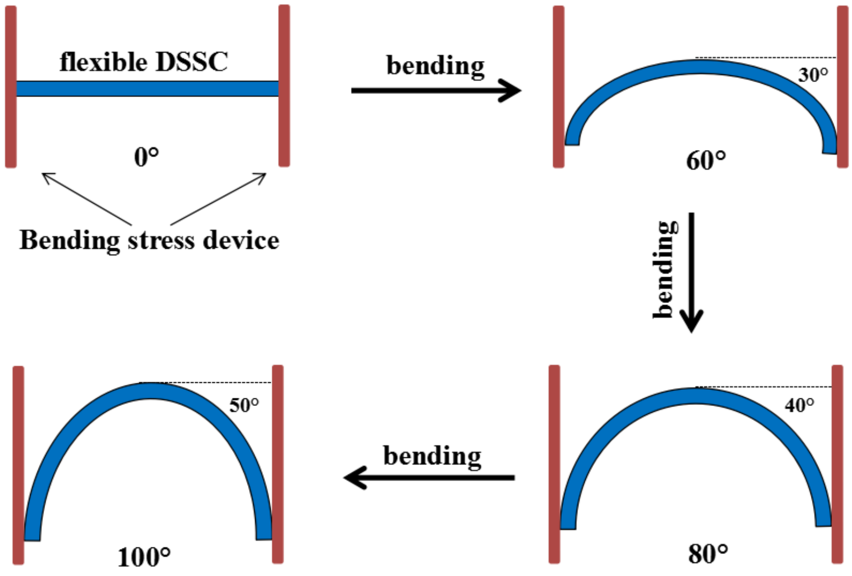

Fig. S6. Schematic of the fully flexible DSSC under different bending stress angles.

The bending stress test is an important parameter for fully flexible DSSCs. So, photovoltaic performance measurement of the flexible DSSC under different bending stress angles (0, 60, 80, 100°) was performed. Fig. S6 gave the schematic of flexible DSSC under different bending stress angle. The fully flexible DSSCs can retain about 97% of its original efficiency under 100° bending stress angle and the corresponding performance parameters were summarized in Fig. S7 and Table S5.

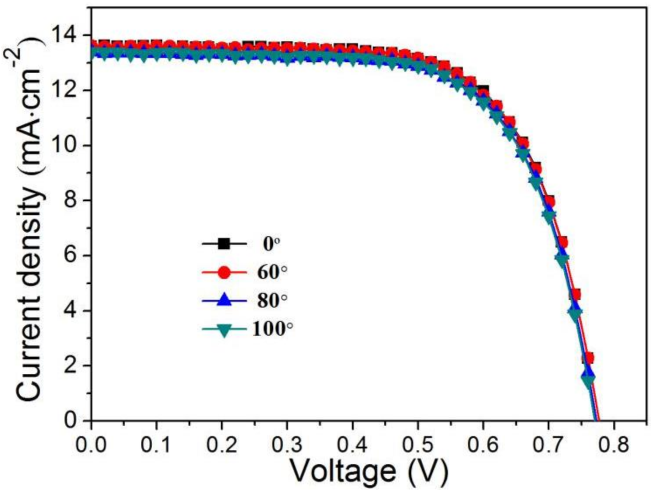

Fig. S7. Current-voltage characteristics of the flexible DSSCs under different bending stress angles.

Table S5. Photoelectric property parameters of the flexible DSSCs based on different bending stress angles.

Bending angles (°)	J_{sc} (mA·cm^{-2})	V_{oc} (V)	*FF*	η (%)
0	13.60	0.78	0.68	7.20
60	13.58	0.78	0.67	7.16
80	13.40	0.78	0.67	6.99
100	13.39	0.77	0.67	6.98